Total Radiation Losses and Energy Balance for Ohmically Heated Divertor Discharges in ASDEX

E.R.Müller, K.Behringer, H.Niedermeyer

IPP III/74 December 1981

MAX-PLANCK-INSTITUT FÜR PLASMAPHYSIK

8046 GARCHING BEI MÜNCHEN

MAX-PLANCK-INSTITUT FÜR PLASMAPHYSIK

GARCHING BEI MÜNCHEN

Total Radiation Losses and Energy Balance for Ohmically Heated Divertor Discharges in ASDEX

E.R.Müller, K.Behringer, H.Niedermeyer

IPP III/74 December 1981

Die nachstehende Arbeit wurde im Rahmen des Vertrages zwischen dem Max-Planck-Institut für Plasmaphysik und der Europäischen Atomgemeinschaft über die Zusammenarbeit auf dem Gebiete der Plasmaphysik durchgeführt.

IPP III/74

E.R.Müller
K.Behringer
H.Niedermeyer

Total Radiation Losses and Energy Balance of the Ohmically Heated ASDEX Divertor Tokamak

(in English)

Dezember 1981

Abstract

Global energy balances were determined for different types of ohmically heated hydrogen discharges in the ASDEX divertor tokamak. The main radiation sources were identified by means of bolometric and spectroscopic diagnostics. In discharges with a poloidal stainless-steel limiter the total radiation in the main volume was the predominant energy loss channel. The radiation losses from the plasma centre, which are mainly due to iron, were reduced by means of the divertor by more than an order of magnitude to an amount which is only about 5 % of the local heating power. Simultaneously, the volume-integrated total radiation losses were halved to values of between 22 % and 32 % of the total input power. The oxygen still present in divertor discharges was removed by Ti-gettering, resulting in an extremely clean plasma with only 12 % total radiation losses. In high-current ($I_p = 400$ kA) and high-density ($\bar{n}_e = 6 \times 10^{13} cm^{-3}$) ungettered divertor discharges, more than half of the total power losses was dumped on the walls of the divertor chambers by radiation and neutral particles. These bolometrically measured volume power losses can be mainly attributed to neutral hydrogen atoms emitted isotropically from an about 1 cm thick layer of a cold ($T_e \approx T_i \approx 5$ eV) and dense ($\int n_{eDIV} \, x \, dl$ up to $8 \times 10^{13} cm^{-2}$) divertor plasma which is in a regime dominated by inelastic atomic and molecular collisions. The fraction of divertor input power dissipated by these processes scaled nonlinearly with the electron density of the main plasma. The drastic reduction of power deposition on the divertor target plates thus achieved in ASDEX is of great importance for reactor-relevant devices with large power exhaust.

Contents

1. Introduction

Energy balances have been published for tokamaks covering large ranges of size and heating power /1-8/. It was recognized /8/ that with growing machine size the fraction of power losses deposited on the walls by radiation increases drastically. Starting from 2o % (ATC; Ref./1/) values of up to 9o % (PLT in the RD and TR modes; Ref./7/) were attained. This radiation behaviour is assumed to be due to the fact that in devices with larger minor radius volume processes such as radiation make a greater relative contribution to power losses. Because the observed trend would be fatal for future tokamak reactors, techniques of controlling plasma-wall interaction have become more and more important. Such methods are the use of divertors instead of material limiters /9/, cold gas blankets /1o/ and radiation cooling of the edge /11/. Of these concepts only the divertor has been experimentally tested, in the DITE bundle divertor /2/ and the DIVA axisymmetric single-null divertor versions /12/. The results were very encouraging: 1. The power losses to the wall decreased by a factor of two to values of 3o to 4o % of the ohmic input power. 2. The medium and high-Z impurities, such as iron, molybdenum and gold,which constitute the main radiation sources in the plasma centre,were preferentially reduced. One of the main objectives of ASDEX is therefore to continue these studies with a larger tokamak device. It has to be demonstrated that the axisymmetric divertor in ASDEX is highly efficient in reducing the radiation losses, especially those in the plasma centre. Divertor tokamaks of comparable size are PDX /13/ and Doublet III /14/.

One essential feature of divertor action is power diversion, which results in suppression of metallic impurity generation in the main volume. An unexpected but highly gratifying ex-

perimental result in ASDEX is the dissipation of a signifcant fraction of the diverted power by isotropic emission of radiation and neutral particles in the divertor chambers /15/. This recently detected and, under certain conditions, even dominant energy loss channel is of great importance from the viewpoint of designing larger tokamaks: the power losses are distributed over a larger divertor wall area, the heat load on the divertor target plates is reduced, and in devices of reactor size, the occurrence of processes such as sputtering and arcing on the target plates should be drastically reduced.

The experimental arrangement is described in Sec.2. The global energy balances for different types of ohmically heated hydrogen discharges in ASDEX are discussed in Sec.3. The radiation profiles and the main radiation sources are treated in Sec.4. Section 5 deals with emission of radiation and neutral particles as an energy sink in the divertor chambers. The summary and conclusions are presented in Sec.6.

2. The ASDEX device and diagnostics

Figure 1 shows a cross-sectional view of the discharge vessel. Two axisymmetric divertors are located at the top and bottom of the main plasma. The major plasma radius is 1.65 m, and the minor radius 0.40 m. The machine is designed for plasma current pulses of 5oo kA and 5 s duration at a toroidal field of 2.8 T. The vessel wall and the limiters are made of stainless steel, the neutralizer plates of titanium.

Figure 1 also shows some of the diagnostics relevant for the energy balance. The radial profiles of the radiation and neutral particle emission in the main volume are determined by performing a bolometric scan measurement from shot to shot and applying the numerical Abel inversion technique on the assumption of circular plasma symmetry. Several bolometers viewing the whole poloidal plasma cross-section are distributed around the toroidal circumference of the vessel. They verify the reproducibility of discharges and - at least roughly - the toroidal symmetry and provide absolute calibration of the radial profiles. The metal-resistor bolometers are of the type described in Ref. /16/. Bolometers cannot distinguish between the two power loss channels, neutral particles and electromagnetic radiation[+)]. The spectral range of the detected radiation is about 1o Å to 2ooo Å for the main plasma (bolometers with gold coating), and 1o Å to the infrared for the divertor plasma (bolometers with blackened surfaces). Divertor radiation losses differ in all four poloidal divertor zones (UO, LO, UI, LI), but bolometers view only the two outside ones. Extrapolation of the bolometrically measured radiation and neutral particles losses in one zone to the respective losses in all four zones (RAD_{DIV}) is performed by, firstly, determining the relation between the bolometric signal in

[+)] In the following "total radiation" denotes the bolometrically measured energy flux due to electromagnetic radiation and neutral particles.

one zone and corresponding electron line density $\int n_{eDIV} \times dl$ and, secondly, measuring $\int n_{eDIV} \times dl$ in each zone by means of 8 mm microwave interferometers. Several thermocouple arrays distributed over the toroidal circumference of the vessel are mounted on the back of the divertor target plates and provide absolutely calibrated, time-integrated profiles of energy deposition. An infrared scanning camera measures temperature profiles across the front surface of the target plates with high time and space resolution.

3. Global energy balance

3.1 Global energy balance for different discharge types

ASDEX hydrogen discharges with ohmic heating can be classified according to the type of plasma-wall interaction: L = limiter discharges, D = divertor discharges, DP = divertor discharges with Ti-gettering inside the divertor chambers /15/. In order to compare the energy balances of these different types of discharges, ASDEX offers the possibility of changing the type from shot to shot with some of the plasma parameters - such as magnetic field, plasma current, density, position and shape - kept constant. Transition from the L to the D type was achieved by retracting a point limiter with a stainless--steel tip from the separatrix shot by shot. During another series of shots transition from D to DP was realized by evaporating a thin titanium layer on the divertor getter panels before every shot. The shot parameters gradually approach those typical of DP discharges. Figures 2a and b show the global energy balance for the transitions L-D and D-DP.

The difference between the ohmic input power (OH) and the spatially integrated radiation and neutral particle losses in both the main plasma volume (RAD) and the four divertor zones (RAD_{DIV}) can be interpreted as thermal conduction and convection losses to the surfaces of the limiter(L type) or the divertor target plates (D and DP types). Limiter calorimetry was not applied, but in the case of D and DP discharges the measurements with the thermocouple arrays on the target plates confirm the energy balance except for an undetected power of about 5 to 15 % of OH. In this context it should be considered that the thermocouples provide only time-averaged data, that part of the divertor volume cannot be viewed by the bolometers, and that there are indications that the energy losses in the divertor chambers sometimes show deviation from toroidal symmetry. The differences between the energy balances for

the two D discharges depicted in Figs.2a and b are due to the slightly different experimental conditions.

With decreasing plasma-limiter interaction the ohmic input power and the percentage lost by radiation in the main plasma are reduced. At a plasma current of around 25o kA and $\bar{n}_e$ of about $2.8 \times 1o^{13} cm^{-3}$ the percentage radiation losses RAD/OH are halved by the use of the divertor and additional Ti-gettering halves them once more. In D discharges with these parameters 2/3 of the power losses of the main plasma is diverted. On an average, half of this energy flux into the divertor is dumped by isotropic emission of radiation and neutral particles on the walls of the divertor chambers, whereas the remainder is deposited on the divertor target plates. Ti-gettering diminishes the volume energy losses in the divertor at the expense of growing power deposition on the target plates.

In Table 1 sets of plasma parameters representative of the three discharges types at $I_p = 25o$ kA are compiled. It should be stressed that the data of D and DP discharges are obtained with a high reproducibility. Only a relatively short conditioning process of the vacuum vessel has to precede in both cases: e.g. in 25o kA D discharges RAD/OH is typically about 45 % shortly after ventilation of the vessel, then falls off to between 3o and 34 % within about 1oo discharges. By contrast, L discharges prove to be very irreproducible: RAD/OH scatters between 45 and 85 %.

Table I

	L	D	DP
$T_e(0)$ [eV]	76o	57o	56o
$\bar{n}_e$ [1o^{13}cm^{-3}]	1.8	2.8	2.1
Z_{eff}	3.3	1.3	1.o
OH [kW]	38o	29o	234
RAD/OH	64 %	32 %	12 %

3.2 Variation of global energy balance with plasma parameters

Whereas in Figs.2a and b the energy balances of three types of discharges are compared (I_p = 25o kA; q_a = 4.4), Fig. 3 shows the variation of the energy balance of D discharges with $\bar{n}_e$. At a current of 4oo kA (q_a = 2.7) the value of $\bar{n}_e$ during the steady state was increased from shot to shot. The result can be summarized as follows:

- The ohmic heating power OH rises slowly with $\bar{n}_e$ because the electron temperature drops.
- The radiation losses RAD in the main volume are nearly constant over a large $\bar{n}_e$ range owing to two counter-balancing effects (Sec.4).
- The power losses RAD_{DIV} due to emission of radiation and neutral particles in the divertor chambers grow nonlinearly with $\bar{n}_e$. Below $\bar{n}_e \approx 3 \times 1o^{13}cm^{-3}$, the range in which RAD_{DIV} and $\int n_{eDIV} \times dl$ (the electron line density in the divertor) are known, the two quantities are linearly correlated (Sec.5).
- Although the energy flux into the divertor increases when the divertor plasma becomes denser, the power deposition on the target plates drastically decreases.

The variation of the energy balance of D discharges with the plasma current at fixed B_t and $\bar{n}_e$ (Fig.4) is characterized by:

- OH is significantly larger at higher I_p.
- RAD is constant or slightly increases, which means that RAD/OH is reduced from 32 % to 22 % if I_p is raised from I_p = 25o kA (q_a = 4.4) to I_p = 4oo kA (q_a = 2.7).

- RAD_{DIV}/OH is also fairly constant. Considering the data at other current values, too, RAD_{DIV}/OH shows a tendency to decrease somewhat with increasing I_p
- The higher plasma current results in an enlarged fraction of the power deposited on the target plates.

In order to answer the question how the energy balance can be influenced by reducing the radiation losses in the main volume and by optimizing the radiation and neutral particle losses in the divertor chambers, we discuss in the following sections the dominant radiation sources and energy loss mechanisms and their spatial distribution.

4. Total radiation profiles and dominant impurities

4.1 Radiation profiles of different types of discharges

Figure 5a shows the radial distribution of the local power densities of ohmic heating power (P_{OH}) as well as total radiation loss power (P_{RAD}) during the stationary phase of a D discharge; Fig. 5b represents the same quantities, but integrated over the volume of a torus with minor radius r. $P_{OH}(r)$ was obtained from Thomson scattering data by assuming Spitzer resistivity and radially constant Z_{eff}. The profile of P_{RAD}, which is the sum of the power losses by radiation and neutral particle emission, was calculated from bolometric scan measurements performed with a time resolution of about 5o ms and a spatial resolution given by 1o overlapping viewing chords through one plasma half, each of them having a space resolution on the axis of 6 cm. Whereas the P_{OH} profiles for different types of discharges with the same value of q_a vary only in amplitude but insignificantly in shape, the corresponding radiation profiles show pronounced differences (Fig.5c). DL discharges represent an intermediate state between the L and D types: the limiter is positioned at the separatrix, and the divertor multipole currents are switched on. In contrast to the L type the DL discharges are sufficiently reproducible for a scan from shot to shot. Comparison of local radiation losses is only made for discharges during which the sawtooth activity was well developed.

In D discharges the spatial distribution of the total radiation is characterized by nearly vanishing centre radiation and a peripheral radiation layer. $P_{RAD}(r=0)$ is in agreement with the results of USX diodes. Time and space correlation of bolometric with spectroscopic profiles leads to the conclusion that the edge radiation is mainly caused by oxygen VUV line radiation. CX losses may contribute up to 25 % to the volume integrated radiation of D discharges /17/, whereas Fe, N and C radiation are of less importance.

A comparison of the DL with the D radiation profiles shows that with increased plasma-limiter interaction the centre radiation losses grow by about one order of magnitude. The iron content of the plasma calculated from spectroscopically measured VUV line intensities is ten times higher in L than in D discharges, whereas the oxygen content keeps approximately constant. Raising the oxygen concentration of the plasma by other means, e.g. by stopping Ti gettering (DP-D transition), even reduces $P_{RAD}(r=0)$. From all these experimental findings one concludes that iron is the dominant radiation source in the centre of the DL plasma and all the more so in the centre of a L plasma. Along with the higher iron content in DL and L discharges, the limiter showed distinct marks of melting; but it is not quite sure if melting is the permanent source of iron contamination or if this process contributes only occasionally. According to radiation loss calculations based on the corona model (/18,19/ ; a review is given in Ref./2o/) an upper limit of about $2 \times 1o^{-4}$ for the iron content in the centre of the DL plasma can be deduced from $P_{RAD}(r=0)$ of the DL radiation profile if one assumes that only iron radiates in the centre. More detailed calculations using spectroscopic results and taking into account anomalous transport and inward drift processes /21/ yield an iron content of $1o^{-4}$ for L discharges. Both values are in good agreement; code calculations show that oxygen has to be considered, too, for the centre of DL discharges.

In DP discharges Ti gettering reduces the oxygen content of the plasma. This is accompanied by a simultaneous drop of the edge radiation emission by a factor of between 5 and 1o.

4.2 Variation of radiation profiles of D discharges with electron line density $\bar{n}_e$

In contrast to the local radiation losses, the spatially integrated total radiation of D discharges shows a weak dependence on $\bar{n}_e$ when $\bar{n}_e$ was increased during the course of a shot by means of gas puffing. The $\bar{n}_e$ rise time was more than an order

of magnitude longer than the energy confinement time (Figs.6a and b). The merely slight variation of radiation with $\bar{n}_e$ is observed, too, in the case of steady-state $\bar{n}_e$ changed from shot to shot (Fig.3). Considering the time development of the radiation profiles (Fig.6c), the behaviour of the spatially integrated signal is composed of two components:

1. The peak height of the edge radiation, emitted mainly by oxygen, grows linearly with $\bar{n}_e$ (Fig.6d);
2. The centre radiation emission, caused predominantly by iron, declines and the profile turns hollow.

In accordance with these statements the spectroscopically measured line intensity of O VI increases and the Fe XVI line intensity decays. Because the iron radiation does not change much in the T_e range of interest /18-2o/, it is concluded that the iron content in the centre of the D plasma is reduced[+].

On the other hand, if $\bar{n}_e$ decreases after switching off the gas inlet, both the centre radiation emission and the calculated iron content of the plasma go up, whereas the peak value of edge radiation declines. The maximum values of edge radiation as a function of $\bar{n}_e$ for the two cases increase and decrease of $\bar{n}_e$ can be fitted by the same straight line (Fig.6d). It should be noted in this context that the variation of $\bar{n}_e$ is a good measure of the change of local $n_e(r)$ because the density profile keeps its shape in the experiments described here.

[+] Accumulation of impurities on the axis is observed spectroscopically at the very beginning of the discharge (<0.2 s), and this effect may help to explain the 0.2 s radiation profile.

5. Energy dumping by isotropic emission of radiation and neutral particles in the divertor

5.1 Divertor energy balance and its dependence on plasma parameters

Figure 7 represents the divertor energy balance for ungettered discharges. Neglecting heat conduction losses to the wall of the main volume (an assumption which is rather well fulfilled in the case of ASDEX since the plasma-to-wall distance is larger than the plasma fall-off length) the divertor input power INP_{DIV} equals the ohmic heating power OH minus the power losses due to radiation and neutral particle emission in the main volume RAD[+)]. The fraction of INP_{DIV} which is lost by bolometrically measured radiation and neutral particle losses in the divertor RAD_{DIV} rises from 28 to 7o % over the $\bar{n}_e$ range covered in 4oo kA discharges.

In three different experimental cases a linear scaling of RAD_{DIV} with $\int n_{eDIV} \, x \, dl$, varied shot by shot, was observed during the stationary phase of D discharges:

1. $\int n_{eDIV} \, x \, dl$ in one divertor chamber was varied by vertical displacement of the plasma column (Fig. 1o b).

2. $\int n_{eDIV} \, x \, dl$ was varied by screening part of the energy and particle fluxes into the divertor by moving the poloidal limiter toward the separatrix (see Fig. 8).

3. $\int n_{eDIV} \, x \, dl$ was varied by raising $\bar{n}_e$ in the bulk plasma.

[+)] The physical processes providing the input power of the divertor are parallel electron heat conduction and, less important, parallel convective energy losses; the relative contributions of the two input power channels are calculated with a numerical code and are discussed in Ref. /22/.

The function f in the relation

$$RAD_{DIV} = f \times \int n_{eDIV} \times dl$$

depends on I_p, multipole currents, shot type etc. but not on $\int n_{eDIV} \times dl$. The value of f scatters from day to day, indicating that it depends sensitively on some yet unknown parameters such as toroidal symmetry etc..

5.2 Thickness of the divertor radiation layer and order of magnitude of the volume energy losses in the divertor

The thickness of the divertor plasma layer emitting radiation and neutral particles was determined as follows: If the outer wing of the poloidal SS limiter approached the separatrix shot by shot, thus absorbing part of the energy and particle fluxes into the divertor, a steep decay of both RAD_{DIV} (Fig.8) and $\int n_{eDIV} \times dl$ within about 1 cm was observed. The width of the radiating boundary layer[+)] of about 1 cm is in rough agreement with the photographically determined width in the visible part of the spectrum.

The length of about 1 cm also agrees with the width of the energy flux profile in the divertor: An infrared camera[++)] using a rotating prism in front of an infrared detector records 2500 line scans per sec along the poloidal direction of the divertor target plate. The signal of the camera is digitized with 128 samples per line and 11-bit resolution, corresponding to a space resolution on the target plates of 1.5 mm and a temperature resolution of 0.1° C[+++)]. From the temperature rise profiles (Fig.9) the power deposition profiles are calculated by numerical solution of the 2-dimensional heat diffusion equation with the boundary conditions valid for the target plates. The half-width of the power depo-

---

+) A correction was made because the width of the scrape-off layer is slightly larger in the divertor chambers than in the main chamber owing to the spreading of flux surfaces.

++) Type THV 780 from AGA, Sweden

+++) The temperature resolution is given for a black body radiation source.

sition profiles amounts to 1.2 cm /23/ and agrees well with the theoretical value, obtained from the BALDUR transport code including the 1-dimensional self-consistent scrape-off layer model /22/.

Assuming uniform emission in a divertor plasma layer with a width of 1 cm one obtains for 25o kA D discharges with $RAD_{DIV}/OH = 1/3$ local power losses of about 1.5 W/cm^3 due to emission of radiation and neutral particles. This emission is more than an order of magnitude higher than the maximum value in the main plasma (Fig.5c). The important question of radiation sources in the divertor is discussed in the following.

5.3 Sources of bolometrically detected power losses in the divertor chambers

5.3.1 Experimental results

Varying $\int n_{eDIV} \, x \, dl$ in one divertor chamber by vertical displacement of the plasma column, we find a linear relation between bolometrically measured radiation and neutral particle losses and the corresponding electron line density (Fig.1oa,b). From simultaneously performed measurements with a 1 mm thick LiF-window (lower transmission cut-off at 1o4o Å) in front of a divertor bolometer it is concluded that Hα and Lα (1216 Å) radiation contribute less than 1o % to RAD_{DIV} (Fig.1oc).

VUV line radiation emitted by impurities such as oxygen cannot explain the order of magnitude of the measured power losses. This is confirmed by spectroscopic measurements in the divertor covering the visible part of the spectrum. Beside hydrogen (HI) and oxygen lines (O II, O III), lines and bands identified as CI, CII, CIII, TiII, CH, OH radiation were observed, and a rather low electron temperature of several eV can be deduced for the plasma in front of the target plates. There is no correlation either between RAD_{DIV} and the oxygen content of the neutral gas in the divertor determined by mass spectroscopy /24/.

Neutral particles with energies above 1oo eV give no significant contribution to the bolometer signal: during steep decay after the gas inlet is switched off the bolometer signal instantly falls off, whereas the flux of charge exchange neutrals in the divertor with E > 1oo eV increases before it decays /17/.

There are two strong arguments for neutral hydrogen atoms in the 5 eV range as the main energy loss channel to the divertor bolometers:

1. During a D-DP transition from shot to shot (see Fig.2b) the bolometric signal in the divertor of the fourth DP shot is significantly lower than that of the last D shot at the beginning of the discharge; at the end of the discharge the DP signal approaches the D signal (Fig. 11). This qualitative behaviour can only be observed in signals correlated with hydrogen, such as the gas feed rate or the neutral gas pressure in the divertor /24/. It is interpreted as the vanishing efficiency of a thin titanium layer in pumping the hydrogen[+)]. Hydrogen line radiation and neutral particle emission in the 1oo eV range are excluded, however, by the experimental results described above. Consequently, low energetic neutral particles remain as the dominant energy loss source.

2. The second argument is that the magnitude of power losses measured in the divertor by means of bolometers can be explained sufficiently well by molecular and atomic processes of hydrogen if the divertor plasma temperature $T_e \approx T_i$ is assumed to be about 5 eV at an electron line density $\int n_{eDIV} \times dl$ averaged over all four divertor zones of about $3.5 \times 1o^{13} cm^{-2}$. This is now discussed in more detail.

[+)] If the Ti layer on the getter panels is sufficiently thick - after ten or more times of Ti evaporation - the pumping efficiency no longer diminishes during the course of a shot.

5.3.2 Atomic and molecular processes in the divertor plasma layer

In 25o kA ungettered discharges with $\bar{n}_e = 2.8 \times 1o^{13} cm^{-3}$ the electron line densities in the outer and inner divertor zones are different, viz. $\int n_{eDIV} \times dl = 5.3 \times 1o^{13} cm^{-2}$ and $\int n_{eDIV} \times dl = 1.6 \times 1o^{13} cm^{-2}$, respectively. It is assumed that the divertor plasma has a temperature of $T_e \approx T_i \approx 5$ eV, and that it is exposed to a flux of thermal H_2 molecules (from mass spectroscopy: $n_{H_2} \approx 4.5 \times 1o^{12} cm^{-3}$ /24/). The relevant molecular and atomic processes are:

Table II:

			$\langle \sigma v \rangle [cm^3 s^{-1}]$
(A)	Dissociation:	$e^- + H_2 \rightarrow 2\underline{H} + e^-$	$0.4 \times 1o^{-8}$
(B)	Ionization of H_2:	$e^- + H_2 \rightarrow H_2^+ + 2e^-$	$0.09 \times 1o^{-8}$
(C)	Dissociative recombination:	$e^- + H_2^+ \rightarrow H + H^*$	$1.8 \times 1o^{-8}$
(D)	Dissociative excitation:	$e^- + H_2^+ \rightarrow \underline{H} + H^+ + e^-$	$0.8 \times 1o^{-8}$
(E)	Resonant charge exchange (CX):	$\underline{H}^+ + H \rightarrow \underline{H} + H^+$	$1.8 \times 1o^{-8}$
(F)	Ionization of H:	$e^- + H \rightarrow H^+ + 2e^-$	$0.12 \times 1o^{-8}$

The rate coefficients are from Ref. /25/. The molecules are isotropically incident on the surface of the divertor plasma layer with a Maxwellian velocity distribution corresponding to room temperature. The flux of H_2 molecules through a surface element of the plasma layer is given by $1/4 \times n_{H_2} \times \sqrt{8\ kT/(\pi m)} = 2.0 \times 1o^{17}\ H_2/(cm^2\ s)$. From this flux a major fraction - outer zone: 85 % and inner zone: 5o%[+)] - undergoes Franck-Condon dissociation (A) or ionization (B) within the plasma layer. Considering the total area of the plasma layer and summing up over all four divertor zones one obtains a total rate of processes (A) and (B) of $2.4 \times 1o^{22}\ s^{-1}$. Each H atom generated in the Franck-Condon process removes a kinetic energy of 3.3 eV, and during each recombination process $H + H \rightarrow H_2$ at the wall

+) From these values it can be seen that the divertor plasma is in a regime between transparent and opaque for traversing thermal neutral hydrogen molecules

or bolometer the dissociation energy of 4.5 eV/molecule is regained. Ionization of H_2 (B) and subsequent processes (C) or (D), which, like Franck-Condon dissociation (A), also result in neutral H atoms transferring energy from the divertor plasma to the walls, yield power losses (without electromagnetic radiation) of about 15 % of those associated with Franck-Condon dissociation. Ionization of H atoms (F) or attenuation due to elastic scattering does not play an important role outside the plasma layer. To summarize, the power losses of the divertor plasma to the walls by neutral hydrogen atoms originating from Franck-Condon dissociation as well as ionization of H_2 and subsequent processes are about 4o kW.

Resonant CX is an atomic process with a major role in enhancing these power losses. Of the neutral particles produced in the processes discussed above a large fraction undergoes resonant CX before escaping from the plasma layer. Neutrals due to Franck-Condon dissociation have a kinetic energy of 3.3 eV, and they gain an energy of about 4 eV in a CX process ($3/2\ kT \approx 7.5$ eV). From the bolometrically measured 9o kW power losses in the divertor chambers we can ascribe 1o kW to electromagnetic radiation (Sec. 5.3.1) and 4o kW to neutral particles mainly due to Franck-Condon dissociation. Neutral particles provided by resonant CX are thus assumed to account predominantly for the difference of 4o kW.

Dissociative recombination (C) delivers two H atoms, one of them (H^*) being in an excited state. According to the relative probabilities of the various processes listed in Table II, the resulting radiation losses, which are mainly due to $L\alpha$ emission, are between 1o % and 15 % of the total power loses due to neutral particles. Excitation of H atoms, generated in processes (A) to (D), by electron collisions should yield $L\alpha$ radiation losses of similar magnitude. Experimentally, 1o % of the volume power losses in the divertor could be attributed

to Lα radiation.This result is within the error bar of the estimated value.

The H^+ flux from the main plasma volume into the divertor chambers is about $1o^{22}$ H^+/s /26/. The production rate of H^+ by means of processes (A) to (F) is roughly estimated at about $0.5 \times 1o^{22}$ H^+/s. From the 9o kW power deposition on the divertor target plates a particle flux of about $1.7 \times 1o^{22}$ H^+/s can be derived[+]. This sink term is thus consistent with the sum of the two source terms.

[+] 9o kW/(5.8 x 5 eV + 15.8 eV) ≈ 1.7 x 22 s^{-1}; the factor 5.8 is from sheath theory (see Ref./22/);on the plate the sum of the ionization and dissociation energies amounting to 15.8 eV/particle is regained.

6. Discussion and conclusions

Global energy balances, total radiation profiles and dominant radiation sources were investigated for different types of ohmically heated hydrogen discharges in ASDEX. In limiter discharges the poloidal SS limiter is the impurity source most disadvantageous with respect to radiation losses of the plasma. It contaminates the plasma mainly with iron. Radiation losses of about two-thirds of the ohmic input power constitute the predominant energy loss channel in limiter discharges (L type). In DL discharges, an intermediate state between limiter (L) and divertor (D) discharges, the central radiation losses, the major fraction of which can be attributed to iron line radiation, are only slightly smaller than the edge radiation emission.

The axisymmetric divertor in ASDEX reduces RAD/OH, the fraction of input power lost by radiation in the main volume, to between 32 % (250 kA discharge) and 22 % (400 kA discharge). The iron content of the plasma (n_{Fe}/n_e) decreases from 10^{-4} (L type) to 10^{-5} (D type), and the central radiation losses in D discharges are reduced by one order of magnitude compared with DL discharges. The radiation profile of D discharges, hollow in the centre and with a pronounced edge peak, is typical of low-Z contaminated plasmas, the low-Z material being oxygen in the case of ASDEX. The reduction of both the radiation losses by a factor of about 2 and the metallic impurity content of the main plasma by an order of magnitude is based on transferring the plasma-wall interaction from the limiter to the remote and separate divertor chambers, from where impurities have only little chance of reentering the bulk plasma.

In Ti-gettered divertor discharges (DP type) the total radiation losses of the main plasma are further reduced to 12 %.

One gets an extremely clean plasma with an oxygen content ten times less than in D discharges and it is characterized by $Z_{eff} = 1$. The residual "radiation" mainly originates from neutral particle emission due to resonant charge exchange.

Normally, in ASDEX the radial profile of the local ohmic heating power is peaked in the plasma centre (Fig.5a). The central losses due to radiation, by comparison, are negligible in D and DP discharges. The energy losses in the centre of D and DP discharges are dominated by anomalous electron heat conduction (see Ref./27/, where energy confinement and its scaling laws are treated in detail). In these discharge types radiation only becomes an important power loss channel at the periphery of D discharges (Fig.5b).

In ASDEX the percentage power losses due to radiation in the main plasma (RAD/OH) show a weak dependence on $\bar{n}_e$ in the stationary (Fig.3) and in the slowly time varying (Fig.6b) case. This behaviour of total radiation was observed, too, in several other tokamaks (TFR /3/,ORMAK /5/, Doublet III /14/). In ASDEX it is interpreted as the result of two counter-balancing processes during $\bar{n}_e$ increase: firstly, growing edge radiation primarily emitted by oxygen and, secondly, decreasing central radiation mainly due to a lowered iron content. The reduction of metallic impurities in the plasma centre by increasing $\bar{n}_e$ was also reported for Pulsator /3o/, Doublet III /14/ and ALCATOR /28,29/ (more Refs. in /29/). For limiter tokamaks it is generally assumed that the impurity generation is diminished by a lower edge temperature. But improved shielding of the plasma against impurities from the wall or changed plasma transport properties could also play a role in the case of divertor discharges. The question cannot be answered definitely at the moment.

RAD/OH of D discharges can be reduced with increased I_p: the radiation losses decrease from 32 % to 22 % if I_p is raised from 25o kA to 4oo kA. This seems to be correlated with a

lower value of q_a; a similar effect can be obtained with smaller B_T at constant I_p. A comparable result was reported for ORMAK /5/ and DIVA /12/.

In high-current (I_p = 4oo kA) and high-density ($\bar{n}_e = 6 \times 1o^{13} cm^{-3}$) divertor discharges the dominant energy loss channel is constituted by power losses due to isotropic emission of radiation and neutral particles (RAD_{DIV}) in the divertor chambers: RAD_{DIV} attains values of up to 55 % of the ohmic heating power or 7o % of the diverted power. Since the radiation and neutral particle losses are restricted to an about 1 cm thick plasma layer, through which the major part of the diverted energy flows, too, the local power losses in the divertor are relatively high and of the order of several W/cm^3. With the exception of some few cases, RAD_{DIV} scales linearly with the divertor electron line density $\int n_{eDIV} \times dl$, which again grows nonlinearly with the electron line density $\bar{n}_e$ in the main chamber . The decrease of RAD_{DIV}/OH with Ti gettering is correlated with a reduction of $\int n_{eDIV} \times dl$. The dependence of RAD_{DIV}/OH on q_a (variation of I_p at constant B_t) is very weak.

The major fraction - about 9o % - of the volume power losses in the divertor can be attributed to the isotropic emission of neutral hydrogen atoms from a divertor plasma with a temperature $T_e \approx T_i$ of about 5 eV. There is a minor contribution to the power losses from Lα and impurity line radiation. Within the divertor chambers strong interaction exists between the neutral gas background and the cold and dense ($\int n_{eDIV} \times dl$ up to $8 \times 1o^{13} cm^{-2}$) plasma layer due to inelastic molecular and atomic collisions. A physical model of the divertor plasma layer thus has to take into account particle sources and energy sinks. The dominant processes are Franck-Condon dissociation of the thermal H_2 molecules into two H atoms, which subsequently undergo resonant charge exchange with protons.

Parallel to Franck-Condon dissociation, H_2 molecules are ionized to H_2^+ molecules, which partly dissociate into H atoms and H^+ ions and partly into two atoms by means of electron capture. Three results obtained from this simple model - estimation of the volume power losses detectable with bolometers, power losses due to Lα radiation, H^+ particle balance in the divertor - are in good agreement with experimental results[+)]. According to the model, the linear scaling of RAD_{DIV} with $\int n_{eDIV} \times dl$ is mainly based on the fact that the neutral gas density n_o in the divertor and, thus, the flux of thermal H_2 molecules are linearly correlated with $\int n_{eDIV} \times dl$.

In ASDEX the volume power losses cool the plasma in front of the divertor target plates. The plasma temperature stabilizes at a value of about 5 eV: at lower temperature the power losses decrease owing to a rapid decay of rate coefficients for inelastic collisions, at higher temperature power losses increase owing to higher plasma and neutral gas densities in the divertor.

The cold and dense plasma in the divertor chambers protects the target plates and reinforces the beneficial influence of the divertor on the main plasma. The power losses are distributed over a larger divertor wall area, the power deposition on the divertor target plates is decreased and sputtering as well as arcing are reduced. In ASDEX the power deposition density on the target plates is about 25 W/cm^2 (25o kA discharges) and the plasma temperature in front of the target plates is about 5 eV. Both values are comparatively small and are,respectively, well below that critical for handling of heat removal and that representing the threshold energy for sputtering. Thus, volume power losses in the divertor will make a significant contribution to the solution of such problems once higher heating powers have raised the plasma parameters into the critical range.

[+)] The existence of different excited vibrational states of the molecules with different dissociation and ionization rate coefficients may considerably complicate a more detailed quantitative calculation.

ACKNOWLEDGEMENT

The authors wish to acknowledge the continual support of the ASDEX team. They wish to express their thanks to W.Engelhardt and G.Fussmann (spectroscopy), H.Murmann and D.Meisel (Thomson scattering), W.Poschenrieder (mass spectroscopy), G.Siller (microwave interferometry), F.Wagner (neutral particle diagnostics) for making their data available. They are grateful to M.Keilhacker, F.Karger, O.Klüber for encouragement and support. We are grateful for the excellent technical assistence of R.Komen and D.E.Groening.

References

/1/ Hsuan,H., Bol,K., Ellis,R.A., Nucl.Fus.15 (1975) 657

/2/ Paul,J.W.M., Axon,K.B., Burt,J., Craig,A.D., Erents,S.K., et al., in Plasma Physics and Controlled Nuclear Fusion Research (Proc.6th Int.Conf. Berchtesgaden, 1976) Vol.2, IEAE, Vienna (1977) 269

/3/ Equipe TFR, ibid., Vol.1, 35

/4/ Berlizov,A.B., Bobrovskij,G.A., Badgasarov,A.A., Vasin,N.L., Vertiporokh,A.N., et al., ibid.,Vol.1, 3

/5/ Bush,C.E., Lyon,J.F., Wall Power Measurements of Impurity Radiation in ORMAK, Oak Ridge National Laboratory Report ORNL/TM-6148 (1977)

/6/ Arunasalam,V., Barnes,C., Bol,K., Boyd,D., Brau,K., et al., in Proc.8th European Conference on Controlled Fusion and Plasma Physics, Prague, 2 (1977) 17

/7/ Hsuan,H., Arunasalam,V., Bitter,M., Bol,K., Boyd,D., et al., in Heating in Toroidal Plasmas (Proc. Joint Varenna-Grenoble Int.Symp.Grenoble, 1978) Vol.2, Pergamon Press, Oxford (1979) 87

/8/ Edmonds,P.H., England,A.C., Nucl.Fus., 18 (1978) 23

/9/ Spitzer,L.,Jr., Phys.Fluids 1 (1958) 253

/1o/ Engelmann,F., Goedheer,W.J., Nocentini,A., Schüller,F.C., in Plasma Wall Interaction (Proc.Int.Symp.Jülich, 1976) Pergamon Press, Oxford (1977) 627

/11/ Gibson,A., J.Nucl.Mat. 76&77 (1978) 92

/12/ DIVA Group, Nucl.Fus.18 (1978) 1619

/13/ Meade,D., Arunasalam,V., Barnes,C., Bell,M., Bitter,M., et al., in Plasma Physics and Controlled Nuclear Fusion Research (Proc.8th Int.Conf. Brussels,198o) Vol.1, IAEA, Vienna (1981) 665

/14/ Nagami,M., Fujisawa,N., Ioki,K., Kitsunezaki,A., Konoshima,S., et al., ibid., Vol. 2, 367

/15/ Keilhacker,M., Albert,D.B., Behringer,K., Behrisch,R., Engelhardt,W., et al., ibid., Vol.2, 351

/16/ Müller, E.R., Design Study of Bolometric Scan Diagnostics for JET, Max-Planck-Institut für Plasmaphysik Report IPP III/56, Garching (198o)

/17/ Wagner, F., Max-Planck-Institut für Plasmaphysik Garching, private communication (1981)

/18/ Jensen, R.V., Post, D.E., Grasberger, W.H., Tarter,C.B., Lokke, W.A., Nucl.Fus. 17 (1977) 1187

/19/ Breton, C., DeMichelis, G., Mattioli, M., J.Quant.Spectrosc. Radiat.Transfer 19 (1978) 367

/2o/ DeMichelis, G., Mattioli, M., Nucl.Fus. 21 (1981) 677

/21/ Behringer, K., Engelhardt, W., Fußmann, G., in Proceedings of the IAEA Technical Committee Meeting on Divertors and Impurity Control, Garching (1981) 42

/22/ Becker, G., Singer, C.E., ibid., 63

/23/ Bein, B.K., Müller, E.R., ibid., 7o

/24/ Poschenrieder, W., Max-Planck-Institut für Plasmaphysik Garching, private communication (1981)

/25/ Heifetz, D., Post, D., Petravic, M., Weisheit, J., Bateman,G., to be published in J.Comp.Phys.

/26/ ASDEX team,presented by F.Wagner, in Proceedings of the IAEA Technical Committee Meeting on Divertors and Impurity Control, Garching (1981) 4o

/27/ Klüber, O., Murmann, H., Energy Confinement in the Tokamak Devices ASDEX and Pulsator, Max-Planck-Institut für Plasmaphysik Report IPP III/72, Garching (1981)

/28/ Scatturo, L.S., Pickrell, M.M., Nucl.Fus. 2o (198o) 572

/29/ Petrasso, R., Gerassimenko, M., Seguin, F.H., Krogstadt,R., Marmar, E., Nucl.Fus. 21 (1981) 881

/3o/ Engelhardt,W., Klüber,O., Meisel,D., Murmann,H., Sesnic,S. et al., in Plasma Physics and Controlled Nuclear Fusion Research (Proc.7th Int.Conf.Innsbruck, 1978)Vol.1, IAEA, Vienna (1979) 123.

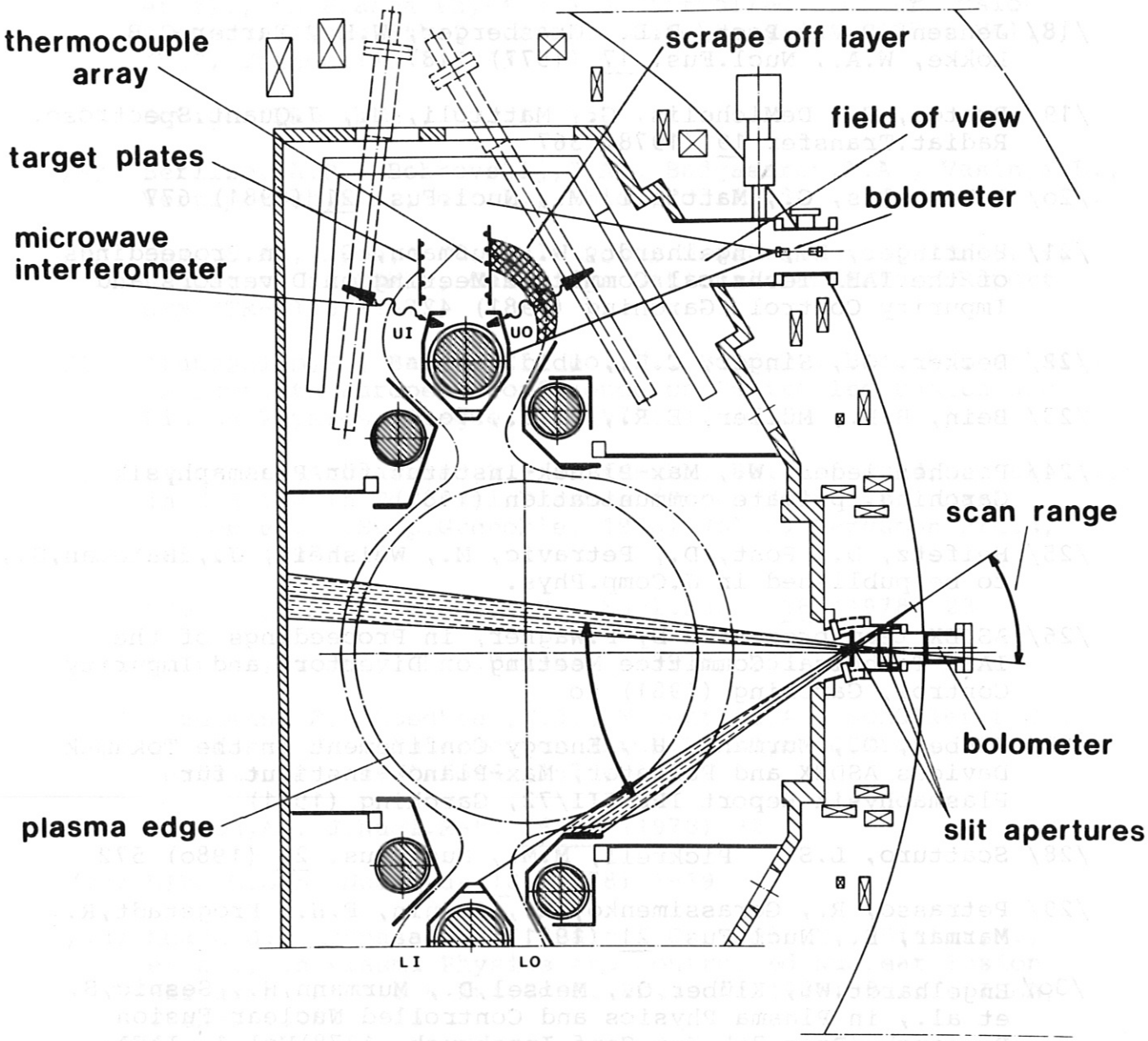

Fig.1: Cross-sectional view of the ASDEX vessel with arrangement of diagnostics relevant for energy balance.

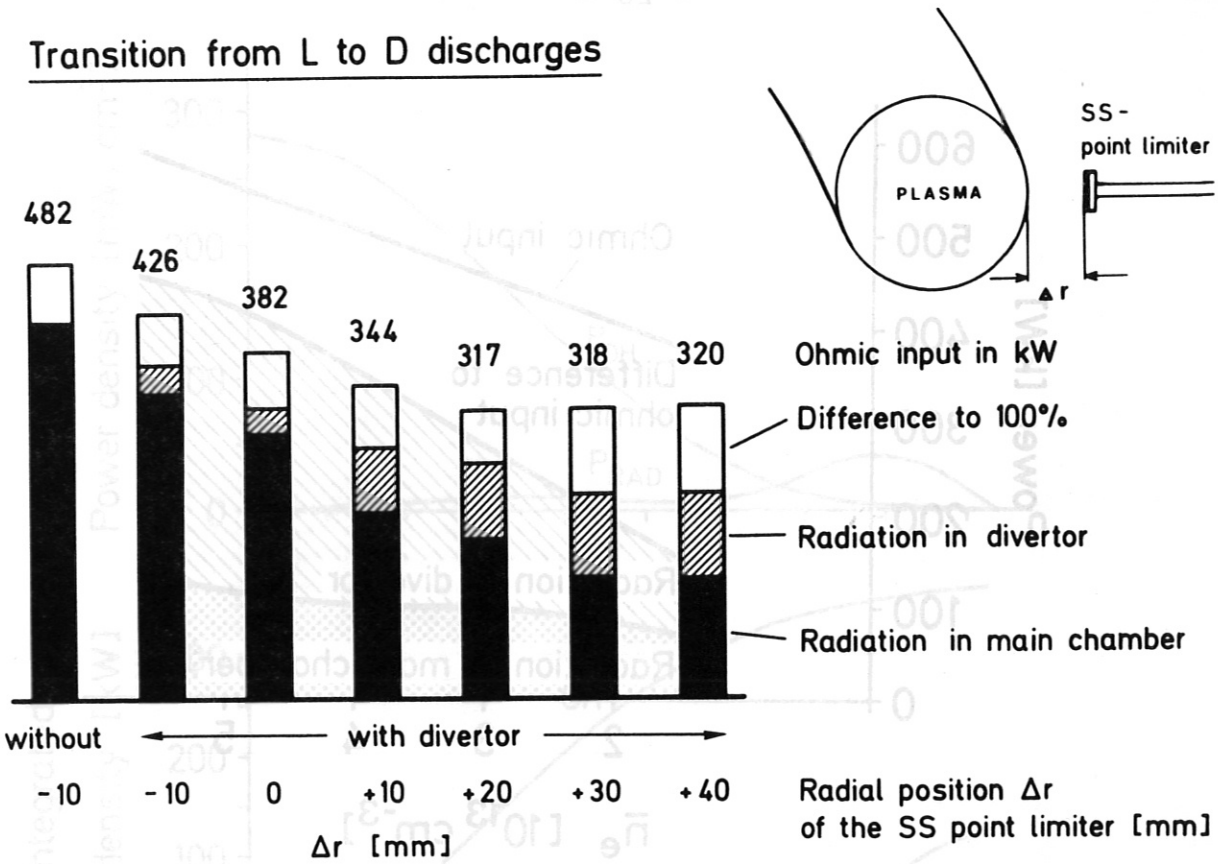

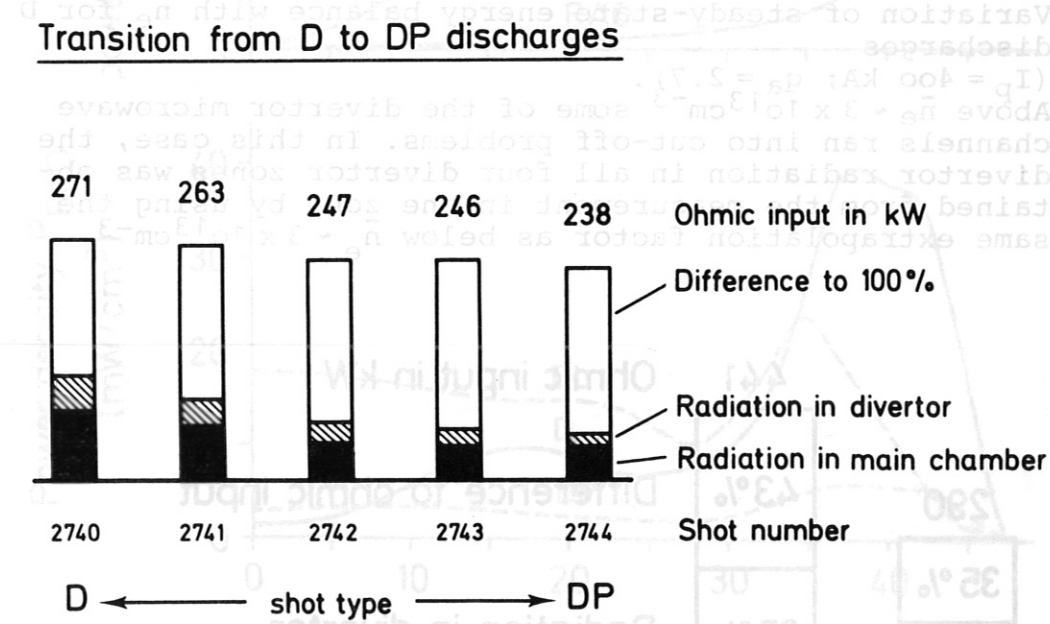

Fig.2a: Steady-state energy balance for a transition from L to D discharges. The radial distance Δr of the point limiter to the separatrix was increased shot by shot (I_p = 275 kA; $\bar{n}_e = 2.3 \times 10^{13}$ cm^{-3}; q_a = 3.9).

2b: Steady-state energy balance for a transition from D to DP discharges (I_p = 250 kA; $\bar{n}_e = 2.8 \times 10^{13}$ cm^{-3}; q_a = 4.3).

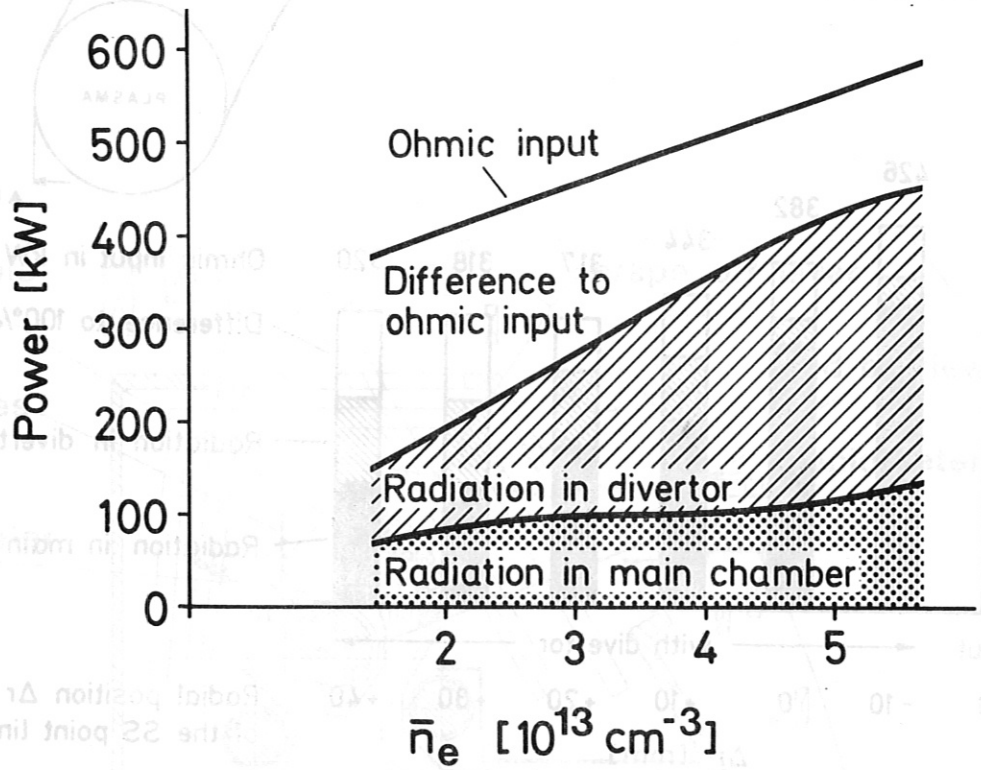

Fig.3: Variation of steady-state energy balance with $\bar{n}_e$ for D discharges
(I_p = 400 kA; q_a = 2.7).
Above $\bar{n}_e \sim 3 \times 10^{13}$cm^{-3} some of the divertor microwave channels ran into cut-off problems. In this case, the divertor radiation in all four divertor zones was obtained from the measurement in one zone by using the same extrapolation factor as below $\bar{n}_e \sim 3 \times 10^{13}$cm^{-3}.

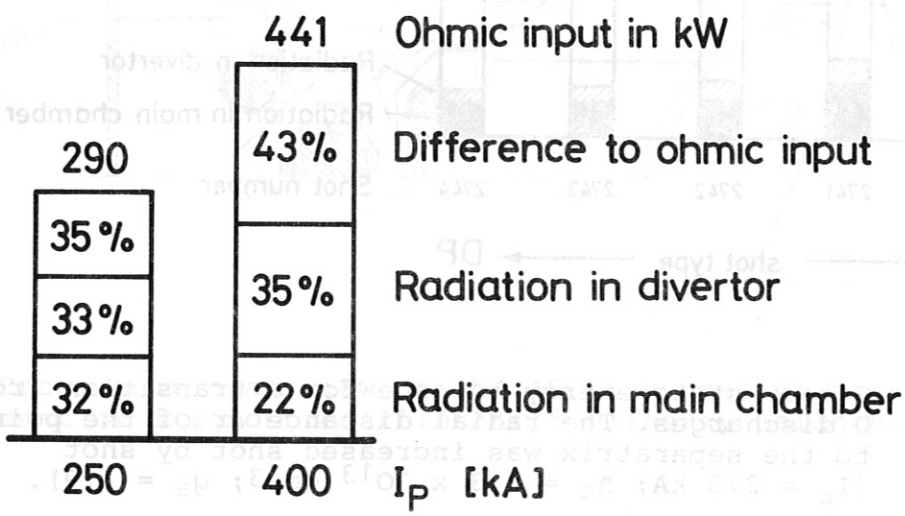

Fig.4: Variation of steady-state energy balance with I_p at fixed B_t for D discharges
($\bar{n}_e$ = 2.8 x 10^{13} cm^{-3}; B_t = 2.2 T).

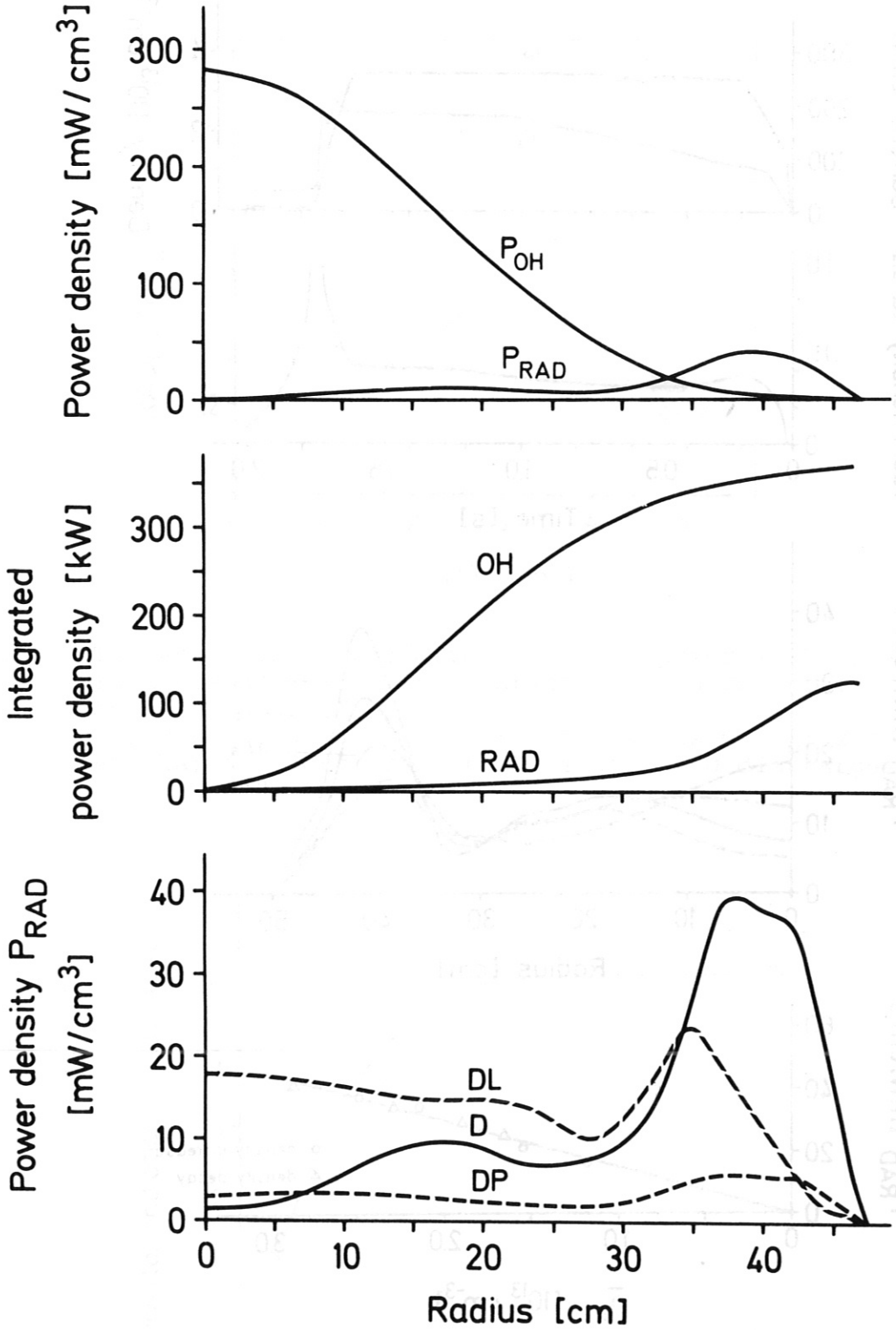

Fig.5a: Radial profiles of both local ohmic heating power $P_{OH}(r)$ and local radiation emission $P_{RAD}(r)$ including charge exchange losses during the stationary phase of D discharges.

5b: $P_{OH}(r)$ and $P_{RAD}(r)$ integrated over the volume of a torus with minor radius r.

5c: Comparison of the total radiation profiles of different discharge types
(I_p = 250 kA; $\bar{n}_e = 3.0 \times 10^{13}$ cm^{-3}; in the case of DP is $\bar{n}_e = 2.3 \times 10^{13}$ cm^{-3}).

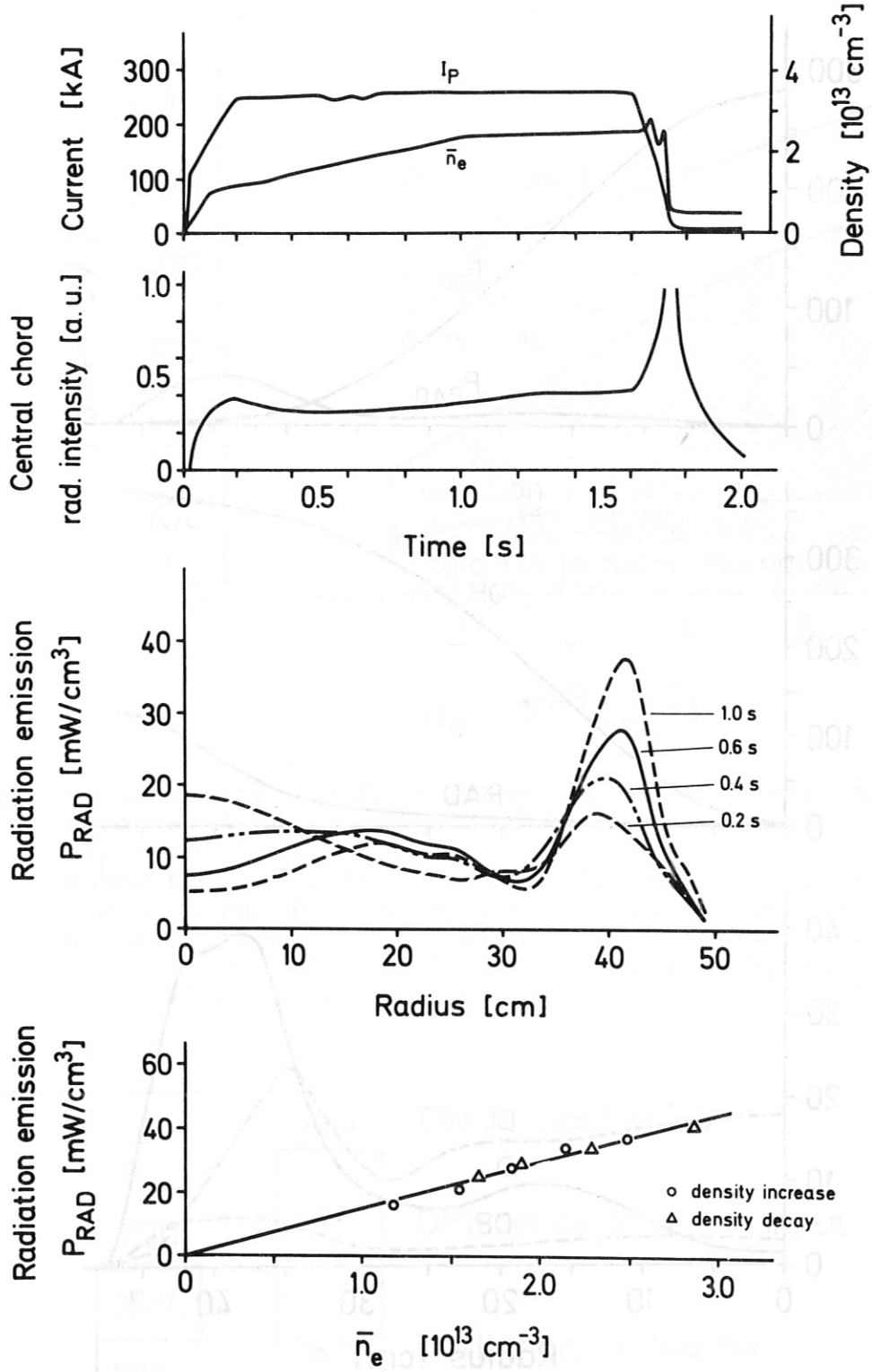

Fig.6a: I_p and $\bar{n}_e$ during a D discharge (q_a = 4.4).

6b: Total radiation emission along the central chord during the course of the shot.

6c: Time development of total radiation profiles

6d: Correlation of the peak height of the edge radiation emission with $\bar{n}_e$. The data points for density decay are taken from another series of D shots in which the gas inlet was switched off (discharge parameters: see Fig. 5).

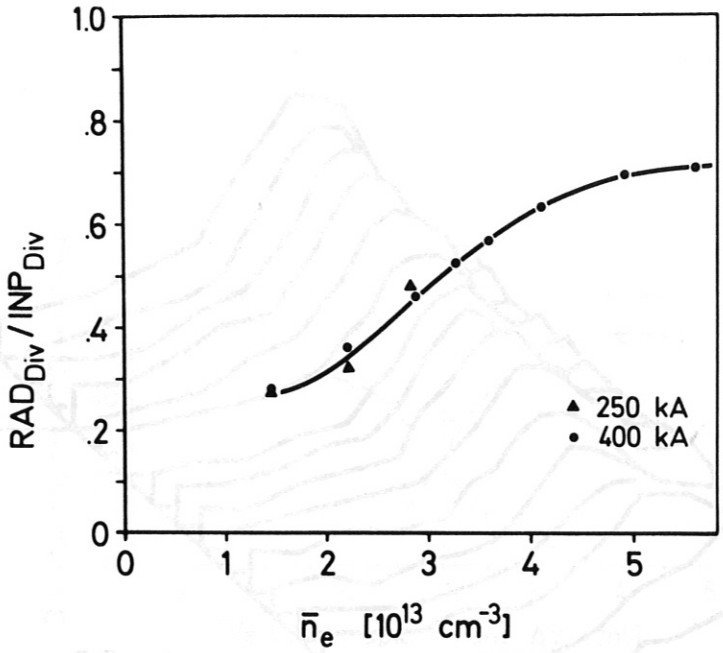

Fig.7: The fraction of the divertor input power (INP_{DIV}) which is lost via emission of radiation and neutral particles (RAD_{DIV}) as a function of $\bar{n}_e$.
(B_t was fixed at 2.2 T for both values of I_p: 250 kA and 400 kA; data are from steady-state of D discharges).

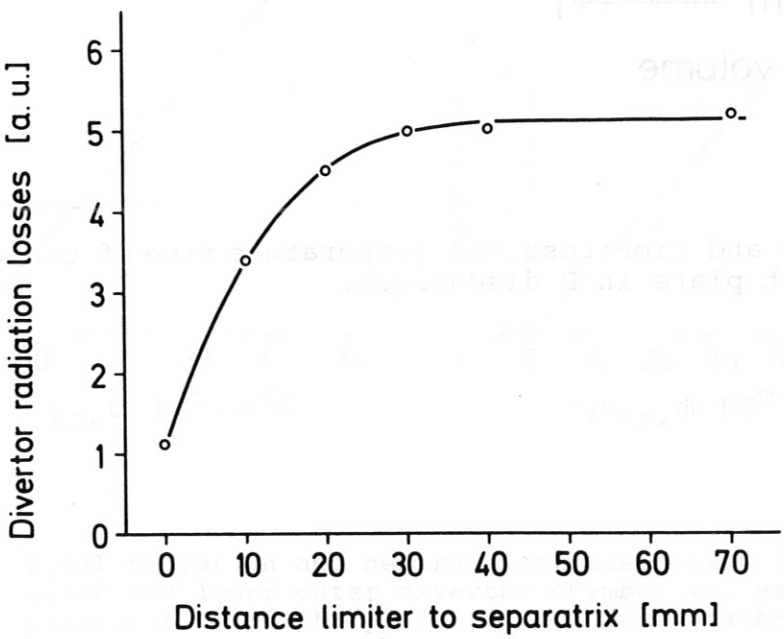

Fig.8: Total power losses by radiation and neutral particles in the divertor chambers for different positions of the outer wing of the poloidal SS-limiter.
(I_p = 250 kA; $\bar{n}_e$ = 2.6 x 10^{13} cm^{-3}; q_a = 4.4).

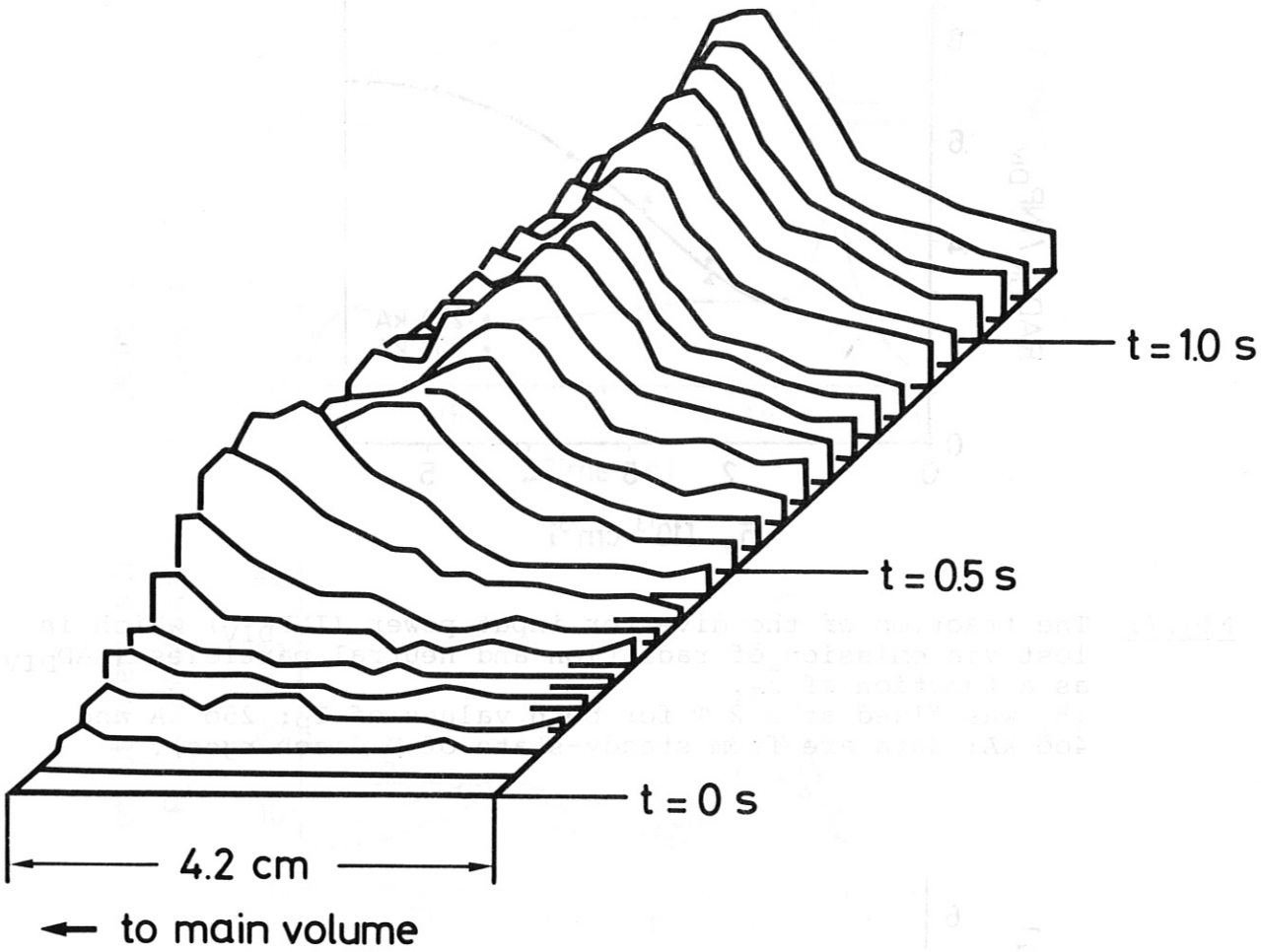

Fig.9: Space and time-resolved temperature rise of one divertor target plate in D discharges.

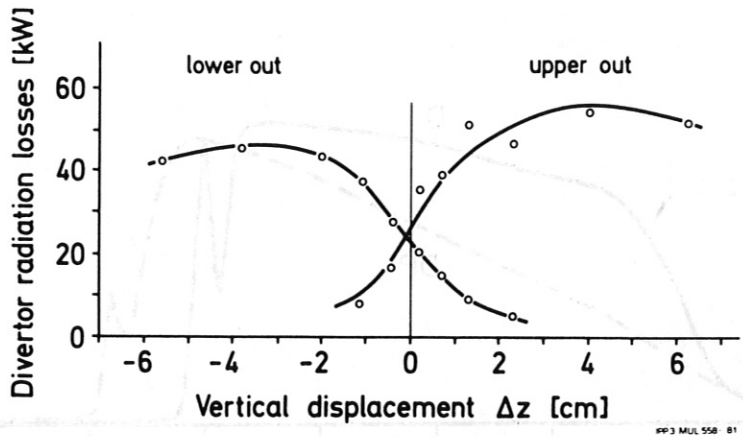

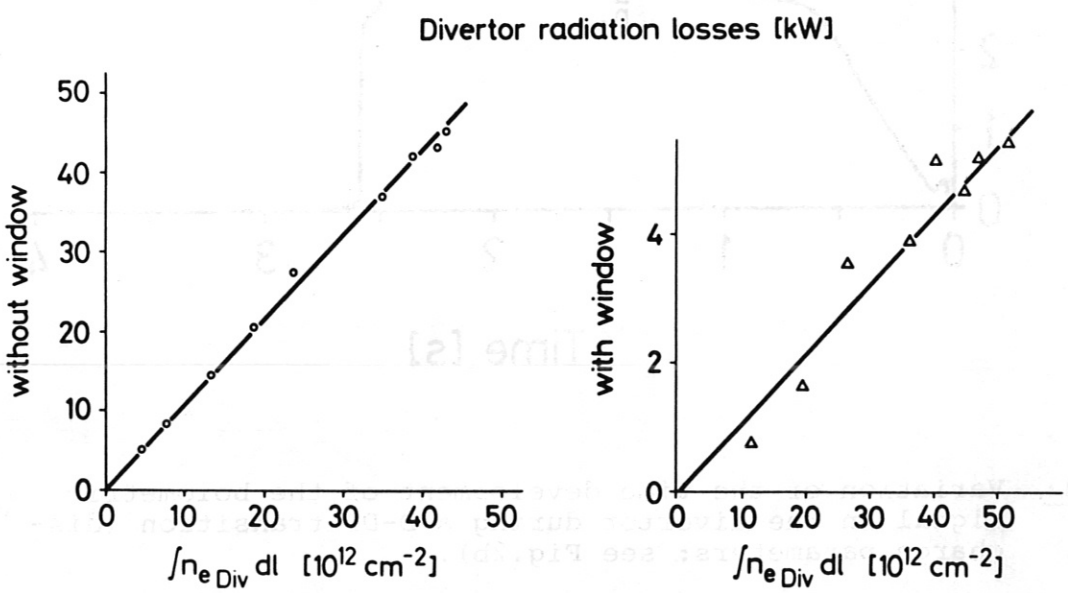

Fig.10a: Total radiation and neutral particle losses in the upper outer and lower outer divertor chamber vs. vertical displacement Δz of the plasma column in D discharges.

10b: Scaling of the radiation and neutral particle losses in one divertor chamber with the corresponding electron line density varied by vertical plasma displacement.

10c: Reduction of the bolometric signal by means of a 1 mm thick LiF window
(I_p = 250 kA; $\bar{n}_e$ = 2.0 x 10^{13} cm^{-3}; q_a = 4.4).

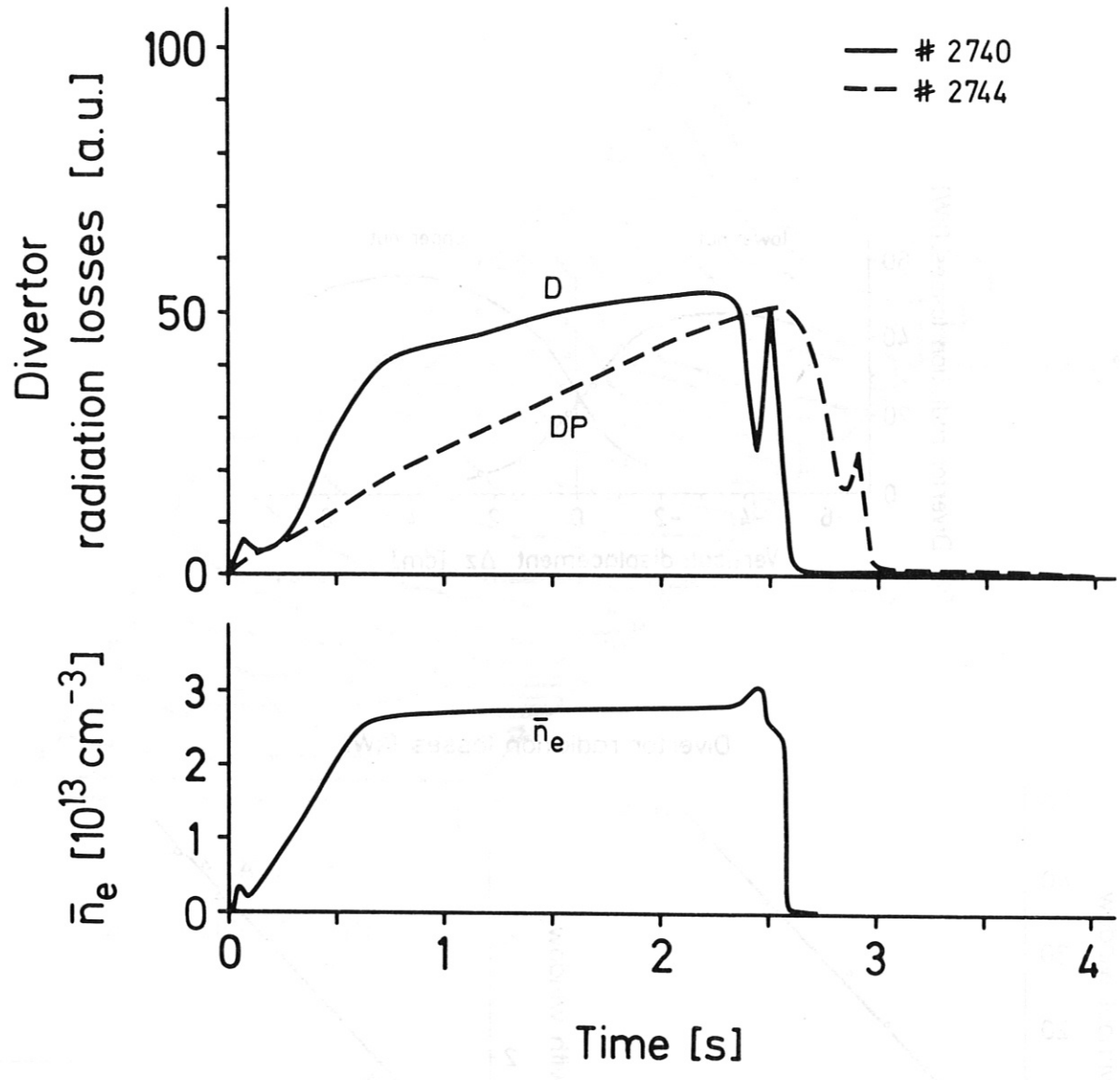

Fig.11: Variation of the time development of the bolometric signal in the divertor during a D-DP transition (discharge parameters: see Fig.2b).